Drug Design, Development and Therapy

Dovepress
Taylor & Francis Group

Open Access Full Text Article

ORIGINAL RESEARCH

Exploration of Key Genes and Molecular Mechanisms in Mice with Perioperative Neurocognitive Disorders Treated with Remimazolam Based on Transcriptomics and Experimental Verification

Shilin Yu[1,*], Bo Chen[2,*], Mei Zhang[3,*], Rong Hu[1], Jin Luo[1], Ju Li[1], Wen Hu[3], Xiaohua Zou[3]

[1]Department of Anesthesiology, The Second People's Hospital of Guiyang, Guiyang, Guizhou, People's Republic of China; [2]Department of Anesthesiology, People's Hospital of Fenggang County, Zunyi, Guizhou, People's Republic of China; [3]Department of Anesthesiology, The Affiliated Hospital of Guizhou Medical University, Guiyang, Guizhou, People's Republic of China

*These authors contributed equally to this work

Correspondence: Wen Hu; Xiaohua Zou, Department of Anesthesiology, The Affiliated Hospital of Guizhou Medical University, Guiyang, Guizhou, People's Republic of China, Tel +86-15120146198; +86-13809416036, Fax +86-851-86771013, Email huwen1997414@sina.com; zouxiaohuazxh@163.com

Background: As the number of elderly patients grew, perioperative neurocognitive disorder (PND) from drug - induced anesthesia and surgery drew more attention. Studies showed remimazolam could reduce PND. Thus, exploring key target genes in remimazolam's intervention of PND was crucial.

Methods: In this study, behavioral observations were conducted using the PND model. Hippocampal tissues from 15 mice (5 PND, 5 PND, and 5 intervention groups) were collected for total RNA extraction and mRNA sequencing. Candidate genes were identified via differential expression analysis and intersection. Key genes were determined through overlapping three algorithms in protein-protein interaction (PPI) analysis and expression verification. Functional enrichment, immune infiltration, and molecular docking analyses were performed, with their expression levels further validated by reverse transcription-quantitative polymerase chain reaction (RT-qPCR).

Results: There were significant differences in the behavior of mice among different groups. Based on the intersection of up-and down-regulated genes in 357 differentially expressed genes1 (DEGs1) and 323 DEGs2, a total of 38 candidate genes were identified. Finally, we selected *Jph3* and *Caly* as the key genes for subsequent study. Moreover, the PCR results showed that the expression of key genes in the PNG group was nearly twice that of the control group ($p < 0.05$). In-depth research revealed that pathways like glutamate receptor binding, tau protein binding, and GABA-gated chloride ion channel activity played important roles in disease occurrence. Meanwhile, 5 immune cells (including dendritic cells, macrophages, and gamma delta T cells) showed substantial differences between the model and PND groups, potentially contributing to disease development. Additionally, only Jph3 was regulated by mmu-miR -6969-5p and mmu-miR-186-5p. Both Jph3 and Caly had good binding abilities with remimazolam (< −5.0 kcal/mol), highlighting their potential as therapeutic agents for PND.

Conclusion: This study identified 2 validated key genes (Jph3 and Caly), providing potential therapeutic targets for PND patients.

Keywords: Cognitive dysfunction, Postoperative cognitive complications, Neuropsychological tests, Remimazolam, Transcriptomics

Introduction

Perioperative neurocognitive disorder (PND) involves cognitive alterations that may happen prior to and/or following surgery. Such changes might encompass cognitive decline prior to surgery, delirium occurring post-surgery, delayed neurocognitive recovery, and cognitive dysfunction after surgery, with symptoms including memory problems, mood disturbances, anxiety, and personality changes.[1] Clinical research has demonstrated that a range of surgical interventions

Received: 11 June 2025
Accepted: 2 September 2025
Published: 10 September 2025

are linked to an elevated risk of PND, with joint replacement following hip fracture exemplifying this association. For example, a cohort study focusing on patients aged over 80 years with hip fractures revealed that the incidence of PND within 30 days post-surgery was as high as 45%, and this was significantly correlated with increased mortality within one year.[2] PND predominantly affects elderly population (individuals over the age of 65) and contributes to increased hospitalization rates, mortality and escalating healthcare costs.[3] Pathological investigations have uncovered several PND traits, such as hippocampal neuroinflammation, neurotransmitter and synaptic issues, blood-brain barrier compromise, oxidative stress, and harm to neurons.[4–7] Among the proposed mechanisms underlying PND, surgery-induced inflammatory responses represent a particularly promising area of research.[8] Notably, a significant study conducted by the Glumac team demonstrated that preoperative administration of corticosteroids mitigates the inflammatory response triggered by surgery, thereby reducing the incidence and severity of cognitive impairment.[9] Despite these insights, the precise mechanisms underlying PND remain poorly understood, and there is an absence of effective preventive or therapeutic strategies are lacking. Anesthetics, particularly benzodiazepines, have emerged as important contributors to PND, with increasing evidence highlighting their effects on cognitive function.[10,11] Given the widespread use of benzodiazepines in the perioperative setting, further investigation is essential to identify key genes associated with their use and the development of PND. Understanding the molecular mechanisms and identifying potential therapeutic targets are crucial for creating more effective treatments for this debilitating condition.

Remimazolam is a novel, rapidly acting benzodiazepine that attaches to GABA receptors in the central nervous system, resulting in sedative and anesthetic effects.[12] As a general anesthetic, remimazolam has recently been the subject of much attention for its ability to alter cognitive function during the perioperative period. Numerous clinical studies have shown that perioperative administration of remimazolam for induction and maintenance of anaesthesia may facilitate the recovery of postoperative neurocognitive function in elderly patients, possibly due to its ability to attenuate inflammatory responses.[11,13,14] In research, remimazolam reduced neurological harm in rats following deep hypothermic circulatory arrest by blocking the HMGB1-TLR4-NF-κB signaling pathway, which enhanced memory and learning skills.[15] Moreover, remimazolam can enhance the expression of α7nAChR, Cyto-Nrf2, HO-1, and proteins related to cognition (CREB, BDNF, PSD95), reduce M1 microglia, improve neuroinflammation or systemic inflammation, and counteract cognitive impairment.[16] These findings suggest that remimazolam not only provides significant clinical benefits in anesthesia and sedation but may also play a pivotal role in neuroprotection. Nonetheless, direct interactions between remimazolam and genes associated with PND, including validation at the molecular docking level, have not yet been documented. This lack of evidence constrains our comprehension of its specific therapeutic mechanisms. Consequently, identifying the key target genes implicated in remimazolam-mediated intervention in PND and elucidating the associated molecular pathways constitute significant gaps that require attention in ongoing research.

In this study, we utilized hippocampal transcriptome sequencing data from an aged mouse model of PND and performed comprehensive bioinformatic analyses, including PPI network construction, expression profiling, functional enrichment, immune infiltration, GeneMANIA analysis, m6A modification assessment, regulatory network mapping, and molecular docking. Through these approaches, we identified key genes associated with the alleviation of PND by remimazolam administered during surgery and explored their potential molecular mechanisms. These findings provide a robust basis for elucidating the molecular underpinnings of remimazolam's neuroprotective effects and for guiding the development of novel therapeutic strategies aimed at reducing PND incidence and enabling personalised treatment. We hypothesize that remimazolam mitigates PND in aged mice by modulating specific target genes, particularly those involved in synaptic function and inflammatory responses, and that alterations in the expression of these genes are closely linked to surgery-induced neuroinflammation and synaptic injury. By identifying these critical targets and delineating their associated pathways, the present study addresses an important gap in current knowledge, as the direct molecular targets of remimazolam in PND—and their connections to surgical stress–related pathways—have not been systematically characterized to date. Integrating transcriptomic profiling with experimental validation, this research aims to clarify the mechanistic basis of remimazolam's effects and to inform future translational applications.

Materials and Methods

Construction of Perioperative Neurocognitive Dysfunction (PND) Mouse Model

The construction of the animal model for this study was conducted at the Animal Center of Guizhou Medical University in Guiyang, China, spanning the period from July 2024 to July 2025. Subsequent research was conducted based on transcriptome sequencing data of the animal model, combined with bioinformatics analysis and experimental verification. A selection of 15 male C57 mice, each weighing between 25g and 35g and aged 18 months, was made. The core rationale for selecting mice at this age is that they can effectively simulate the physiological state of elderly patients (> 65 years old), and advanced age is the most important clinical risk factor for PND in humans.[17] These SPF-grade mice were obtained from Jinan Pengyue Laboratory Animal Breeding Co. Ltd, with the production license number SCXK (Lu) 2022–0006. Approval for the experimental protocol (2403666) was granted by the Animal Center of Guizhou Medical University, with all procedures conducted in accordance with the National Institutes of Health Guide for the Care and Use of Laboratory Animals. Following a week of regular feeding, the mice were divided randomly into three groups: PND group (5 mice), model group (5 mice), and intervention group (5 mice).[18–20] The mice in the PND group were anesthetized, underwent a median opening, and received lidocaine gel paste for pain relief, without any additional surgical procedures or treatments. In the model group, the mice were put under anesthesia using sevoflurane (2–3%, 1 L/min) and positioned on a warming mat, after median opening, the intestinal tract was exposed, and microvascular clips were applied to the superior mesenteric artery to constrict it and closed for 20 min, and the clips were loosened.[21,22] After the clip was released, the bowel was put back into the abdominal cavity, and 0.25% ropivacaine was infiltrated into the abdominal wall along the incision, and then the operative incision was joined together with a sterile suture. The surgical procedures performed on the mice in the intervention group were similar to those on the mice in the model group. Prior to surgery, they were given remimazolam through a tail-vein injection at a dose of 10mg/kg.[16] After being anesthetized, the mice were euthanized, and their hippocampal tissues were collected. All cognitive tests were performed in well-lit environments.

Sample Collection

In this study, 15 hippocampal tissue samples from 3 groups of mice in the mouse model were collected for RNA sequencing. Three groups were formed from these samples: the model group, the intervention group, and the PND group.

RNA Sequencing and Data Preprocessing

We extracted total RNA from 15 hippocampal tissue samples using TRIzol (Invitrogen, CA, USA). Following this, the NanoDrop ND - 1000 spectrophotometer (NanoDrop, Wilmington, DE, USA) was employed to measure the total RNA's amount and integrity, and the Bioanalyzer 2100 system (Agilent, CA, USA) was used as well. To be suitable for subsequent experiments, samples had to meet the criteria of concentrations over 50 ng/μL, RIN values more than 7.0, OD 260/280 ratios surpassing 1.8, and total RNA greater than 1 μg. Using Dynabeads Oligo (dT)25–61005 (Thermo Fisher, CA, USA), Poly(A) RNA was isolated from 1 μg of total RNA with a two-round purification method. Afterward, the poly(A) RNA was fragmented into smaller parts using the Magnesium RNA Fragmentation Module (NEB, cat. e6150, USA) at 94°C for 5 to 7 minutes. The RNA fragments that were cleaved were transcribed back into cDNA with the help of SuperScript™ II Reverse Transcriptase (Invitrogen, cat. 1896649, USA). The Polymerase Chain Reaction (PCR) amplification was conducted with these conditions: Initially, a denaturation step was executed at 95°C for 3 minutes. Afterward, 8 cycles were performed, each including denaturation at 98°C for 15 seconds, annealing at 60°C for 15 seconds, and extension at 72°C for 30 seconds, with a final extension at 72°C for 5 minutes. The ultimate cDNA library featured an average insert size of 300 ± 50 base pairs. Sequencing was performed using the Illumina NovaSeq 6000 platform in paired-end 150 bp (PE150) mode. After the sequencing process, Fastqc software (https://www.bioinformatics.babraham.ac.uk/projects/fastqc/) discarded low-quality reads, while Phred software (http://www.phrap.org/phredphrapconsed.html) analyzed AT/GC separation. Additionally, Featurecounts was utilized for quantitative analysis, with a transformation of the counts matrix. The gene expression distribution across samples was visualized using the ggplot2 package (v 3.3.5).[23] Principal component analysis (PCA) was performed on samples from the model (5

mice), intervention (5 mice), and PND groups (5 mice) using the prcomp function in the R package (version 4.2.2) to compare the degree of clustering of the samples between the groups.

Identification of Candidate Genes and Pathway Analyses

To find differentially expressed genes (DEGs) affecting the disease during drug treatments, the DESeq2 package (v 1.34.0)[24] was employed, identifying DEGs with |log2fold change (FC)| > 0 and $p < 0.05$. Specifically, DEGs1 were identified by comparing case samples from model (5 mice) and PND groups (5 mice). DEGs2 were ascertained by comparing case samples from intervention (5 mice) and model group samples (5 mice). Afterward, the ggplot2 package (v 3.3.5) and pheatmap package (v 1.0.12),[25] were utilized to generate a volcano plot and heatmap, respectively, highlighting the top 10 DEGs with the highest up- and down-regulation according to |log2FC|.

Afterward, an analysis was conducted on the functions and signal pathways of DEGs1 and DEGs2 for Gene Ontology (GO) and KEGG enrichment ($p < 0.05$) with the clusterProfiler package (v 4.6.0).[26] The GO terms were divided into three categories: Biological Processes (BPs), Cellular Components (CCs), and Molecular Functions (MFs). Subsequently, the top 5 pathways with significant p-values from GO terms and the top 15 pathways from KEGG were visualized by the enrichplot package (v 1.14.2).[27] Subsequently, in order to find out the genes associated with drug intervention in different groups. Using the VennDiagram package (v 1.7.1), we identified the overlap between genes with elevated expression in DEGs1 and those with reduced expression in DEGs2, as well as the overlap between down-regulated genes in DEGs1 and up-regulated genes in DEGs2[28] and the two overlapping gene sections served as candidate genes related to drug interventions.

Isolation of Key Genes

A PPI network for the candidate genes linked to drug intervention was built using STRING, a tool for retrieving interacting genes/proteins, with an interaction score greater than 0.15. Finally, to visualize the network, the Cytoscape (v 3.7.0)[29] was utilized. Following this, three algorithms in the Molecular Complexity Detection (MCODE) plugin Maximal Clique Centrality (MCC), Density of Maximum Neighborhood Component (DMNC) and Maximum Neighborhood Component (MNC) were used to score the genes in the PPI network and identify candidate key genes by overlapping the top 5 scored genes. MCC evaluated the importance of nodes by identifying all maximum cliques in the network; the larger the maximum clique a node belonged to, the higher its centrality score. This method was able to focus on the most tightly connected gene clusters and explore core modules with highly coordinated functions. DMNC could take both local dense connections and module boundary bridging effects into account, assign higher scores to the inter-module regulatory functions of nodes, and was more suitable for capturing key nodes in modular network structures. MNC had a simple structure and high computational efficiency, making it suitable for quickly screening out genes with high connectivity. To moreover clarify the expression of the candidate key genes, the Wilcoxon test was applied to analyze the differences in the expression levels of the candidate key genes among the model group (5 mice) and the PND group (5 mice), and among the intervention group (5 mice) and the model group (5 mice) ($p<0.05$), and the genes with the opposite expression trends and significant differences in the two comparison groups were selected as the final key genes.

Gene Set Enrichment Analysis (GSEA)

To elucidate the biological functions and pathways of the key genes in the disease process, we first used m5.go.mf.v2024.1.Mm.symbols.gmt and m5.go.bp.v2023.2.Mm.symbols.gmt as the background gene set. Thereafter, with the assistance of the corrplot package (v 0.92) (https://rdrr.io/cran/corrplot/), we calculated the Spearman correlation coefficients of each key gene with all other genes in all samples of the model and intervention group sequencing datasets and sorted the results in descending order. Subsequently, we performed GSEA using the clusterProfiler package and visualized the top 5 results in terms of enrichment scores using the enrichplot package (v 1.14.2) (|normalized enrichment score (NES)| > 1.0, $p < 0.05$ and false discovery rate (FDR) < 0.05).

Gene-Gene Interaction (GGI) Network, m6A Modification and Molecular Regulation Network

Furthermore, to better uncover the biological characteristics and interactions of key genes, the GeneMANIA website (http://genemania.org/) was applied to analyze and construct a GGI network between key genes and other genes. Meanwhile, the Prediction of Mammalian N6-methyladenosine (m6A) Sites Based on Sequence-Derived Features (SRAMP) (http://www.cuilab.cn/sramp/) was used to predict the m6A modification sites of key genes to understand the RNA methylation modification of key genes. Subsequently, with the intention of probing into the regulatory mechanisms of essential genes at the molecular stratum microRNAs (miRNAs) associated with key genes were predicted using the Targetscan database and the miRDB database available on the Home-miRWalk website (https://www.uni-heidelberg.de/). Finally, the visualization of the regulatory network of key gene-miRNAs was achieved using Cytoscape package (v 3.7.0).

Analysis of Immune Infiltration

For the purpose of discerning the variations in immune cells associated with the disease, based on the sequencing data, the immunedeconv package (v 2.1.0)[30] was resorted to explore the percentage of infiltration of 15 immune cells in the samples between the two groups, specifically between the model and PND groups (5 mice) and between the intervention group (5 mice) and the model group (5 mice), and then heatmaps were plotted using the ggplot2 package (v 3.3.5). To further comprehend the disparities in the immune microenvironment among groups, we compared the immune cells that differed significantly between the model and PND groups and between the intervention and model groups using the Wilcoxon test ($p < 0.05$), which was demonstrated by heatmap plotting using the ggplot2 (v 3.3.5), and the correlations between the differential immune cells and key genes were analyzed by the corrplot package (v 0.92) were analyzed ($|$correlation coefficient (cor)$| > 0.3$, $p < 0.05$).

Molecular Docking

To verify the affinity of remazolam for key genes, the three-dimensional architectures of proteins (key genes) and molecular ligands (active ingredients) were obtained from the Protein Data Bank (PDB) at http://www.rcsb.org and the PubChem database at https://pubchem.ncbi.nlm.nih.gov/, respectively. Then proteins and ligands were transferred to the cb-dock online website to perform molecular docking and their free binding energy were calculated. When the binding affinity is lower than −5.0 kcal/mol, it implies that the small ligand molecule binds to the receptor protein spontaneously. Moreover, when the binding affinity is lower than - 7.0 kcal/mol, it suggests that the ligand exhibits favorable binding activity towards the receptor.

Open Field Test

Prepare a mouse experimental box made of medical - grade ABS material with dimensions of length × width × height = 1 m × 1 m × 0.4 m. The experiment comprised three groups: the model group (5 mice), PND groups (5 mice), and the intervention group (5 mice). The color of the base of the box should be made as different as possible from what belongs to the experimental animals. The box's area is generally divided into four corners, the perimeter, and the central area. Software can automatically calculate the activity distance, residence time, entry count, and average speed of the experimental animals in these zones. Specifically, the total horizontal movement distance reflects the locomotion of the mice, the aggregate quantity of entries into the central zone mirrors the anxiety level of the mice, the residence time in the central area reflects the anxiety level of the mice, the quantity of grooming instances mirrors the vertical locomotion of the mice, mainly embodying their exploratory behavior, and the number of feces reflects the anxiety level of the mice.

Morris Water Maze Test (MWM)

The backs of the mice's heads and necks were marked in advance to avoid interference from miscellaneous colors during the experiment. The experiment comprised three groups: the model group (5 mice), PND groups (5 mice), and the intervention group (5 mice). Prior to beginning the experiment, the circular water maze pool was filled with about 30 cm

of water. The escape platform was positioned in the center of a quadrant, 15 cm from the pool's edge and 1 cm beneath the water's surface. Titanium dioxide powder was thoroughly blended into the water to conceal the underwater platform from the test animals, and the water temperature was maintained at 22–24°C. The illumination intensity was maintained at 100–150 lux, with uniform lighting from the top, which did not produce strong shadows or glare. Environmental noise was controlled at a low level to avoid interference with mouse behaviors from sudden noises. ① In the initial phase of the experiment, the mouse was positioned on the platform for 30 seconds to help it recognize extra maze cues. Afterward, a quadrant was chosen at random as the starting point, and the mouse was introduced into the water with its head directed toward the pool wall (the quadrant's center). Researchers recorded the time it took for the mouse to discover the underwater platform, known as the escape latency. The maximum swim time was capped at 60 seconds. If the mouse found the platform within this period, it was immediately removed from the water. If the mouse did not find the platform within 60 seconds, it was gently directed to the platform and given 30 seconds to reorient itself using the distant visual cues. The training was conducted 4 times daily at the same time for 6 days in a row, with the four quadrants being repeated in sequence. Following each training session, the animals were dried and returned to a warm cage to dry off. An automated system captured and analyzed the movement paths of the mice. ② Spatial Probe Experiment: After the surgery on the 7th day, the spatial probe experiment was conducted on the 1st and 2nd days after the surgery to test the mice's learning and memory ability of the escape platform. After 6 consecutive days of place navigation experiment training, the mice had formed a fixed memory of the escape platform. During the spatial probe experiment, the concealed underwater platform was taken away, and the mouse was positioned in the water from the quadrant opposing the one where the initial platform was situated. The proportion of time the mouse spent in the target quadrant over 60 seconds and the frequency of its entries into this quadrant, meaning the percentage of time spent in the target quadrant and the count of entries into the escape platform area, were recorded. These were used as the detection indicators of spatial memory. On the first day after surgical modeling, the MWM test was used to detect cognitive function. Subsequently, according to the experimental design, different groups were given different treatments. In the remimazolam intervention group, the calculated dose of remimazolam was diluted with normal saline according to the mouse's body weight, and then 1 mL was taken for intraperitoneal injection. In the case of the PND group and the PND group, 1 mL of normal saline was directly injected. After treatment, the MWM experiment was conducted to detect cognitive function.

Y - Maze Experiment

First, a Y - maze was self - made. It consisted of three arms of equal length, with an angle of 120 degrees separating each pair of arms. The experiment comprised three groups: the model group (5 mice), PND groups (5 mice), and the intervention group (5 mice). There was a movable partition at each central part, and the inner arms and the bottom of the maze were painted black. Each arm is 35 cm long, 8 cm wide and 15 cm high. The experimental environmental conditions were controlled as follows: Light intensity: maintained at a low light condition of 20–30 lux to reduce the impact of anxiety-like behaviors; Room temperature: controlled at 22 ± 1°C; Noise level: the laboratory environment was kept quiet to avoid interference with animal behaviors from sudden noises. One mouse was located at the tip of an arbitrary arm of the Y - maze and allowed to investigate freely during an 8 - minute period. During the 8 minutes, the behavioral changes of the animal were recorded by a camera system, and the subsequent indicators were noted: (1) The overall quantity of arm entries: The frequency with which the animal entered the maze arms, with the standard that all four feet of the mouse entering an arm counted as one entry. (2) One alternation: It referred to the situation where the mouse successively entered all three arms of the Y - maze in sequence. (3) The highest number of alternations: It was computed as the overall number of arm entries minus 2. The score of spontaneous alternation behavior was computed as (the total number of alternations / the maximum number of alternations) * 100%. In the Y - maze experiment, the detection indicators were recorded by an image acquisition system, and the data were analyzed using SPSS software (v 30.0.0).[31]

Expression Validation of Key Genes

To explore the differences in the expression of key genes in the tissue samples of the control (5 mice), model (5 mice) and intervention groups (5 mice), the dissimilarities in the manifestation of key genes in the samples of the three groups were verified by Reverse Transcription Quantitative Real - Time Polymerase Chain Reaction (RT-qPCR) in the sequencing dataset.

We performed a *t*-test for expression differences between samples ($p < 0.05$). Moreover, the statistical robustness of the sample size of 5 mice per group was verified through power analysis. The expression levels of key genes between samples were tested by $2^{-\Delta\Delta Ct}$. The results were calculated with Graphpad Prism 5 and p-values were calculated. The internal reference gene was GAPDH, which was used to normalize the results (Supplementary Table 1).

Enzyme-Linked Immunosorbent Assay (ELISA)

We measured the serum cytokine levels to study the expression of inflammatory factors in the control group (5 mice), model group (5 mice), and intervention group (5 mice), following the manufacturer's protocol, quantitative ELISA kits were used to evaluate TNF-α and IL-1β. Optical density was measured at 450 nm, followed by determining cytokine concentrations using specific standard curves for each cytokine.

Statistical Analysis

Bioinformatics analyses were carried out utilizing the R language (v 4.2.2). R was designed by Ross Ihaka and Robert Gentleman. The Wilcoxon test was employed to assess the differences between two groups, while the *t* - test was applied to contrast the distinctions among the three groups. A p - value (two-tailed test) of less than 0.05 was regarded as statistically significant.

Results

High Sequencing Quality and Uniform Sample Distribution

Generally, when the Phred score was 30%, the error probability was 0.1%. The data quality control results indicated that the Phred score was generally around 40%, suggesting that the sequencing quality was extremely high (Figure 1A). There was no obvious AT or GC separation in the sequencing data. The overall distribution of gene expression levels was between 0–2.6 (Log_{10}FPKM, showing a relatively even distribution (Figure 1B). Meanwhile, the PCA results showed that the samples among the three groups were well - clustered (Figure 1C).

Evaluation of Animal Models

The experimental timeline for animal model construction is illustrated in Figure 2A and B–D display representative trajectory plots from the Morris water maze (MWM), Y-maze, and open field tests for each group of mice. To evaluate hippocampus-dependent spatial learning and memory, we employed the MWM test, in which mice in the PND group exhibited a reduced number of platform crossings compared to those in the model group, whereas the intervention group showed a significantly higher number of platform crossings than the PND group (Figure 2E). To further assess hippocampal spatial working memory, the Y-maze test was conducted, demonstrating that the PND group made significantly fewer arm entries than the model group, while the intervention group exhibited a marked increase relative

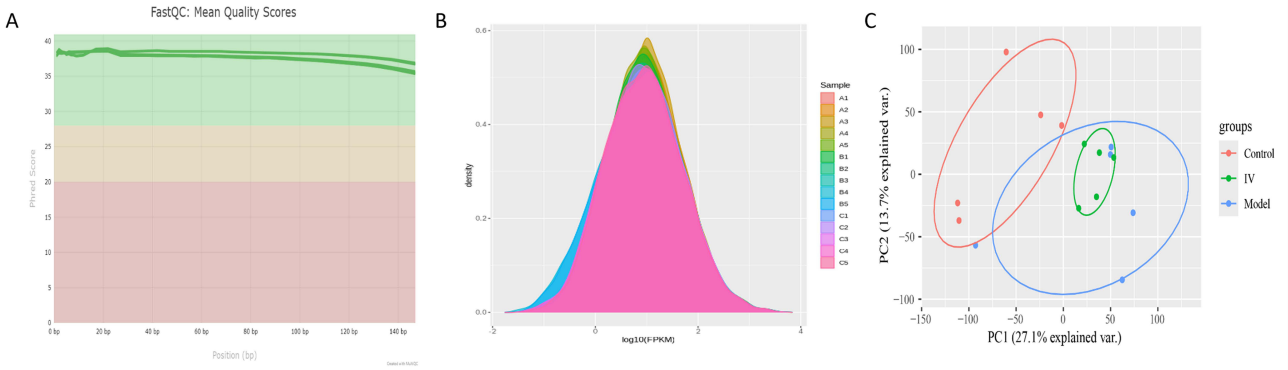

Figure 1 Sequencing data quality and sample distribution. (**A**) The distribution of the mean quality value per base in sequencing reads. (**B**) Density map of gene expression values of different samples. (**C**) PCA, principal components analysis.
Abbreviation: IV, intervention group.

https://doi.org/10.2147/DDDT.S541958

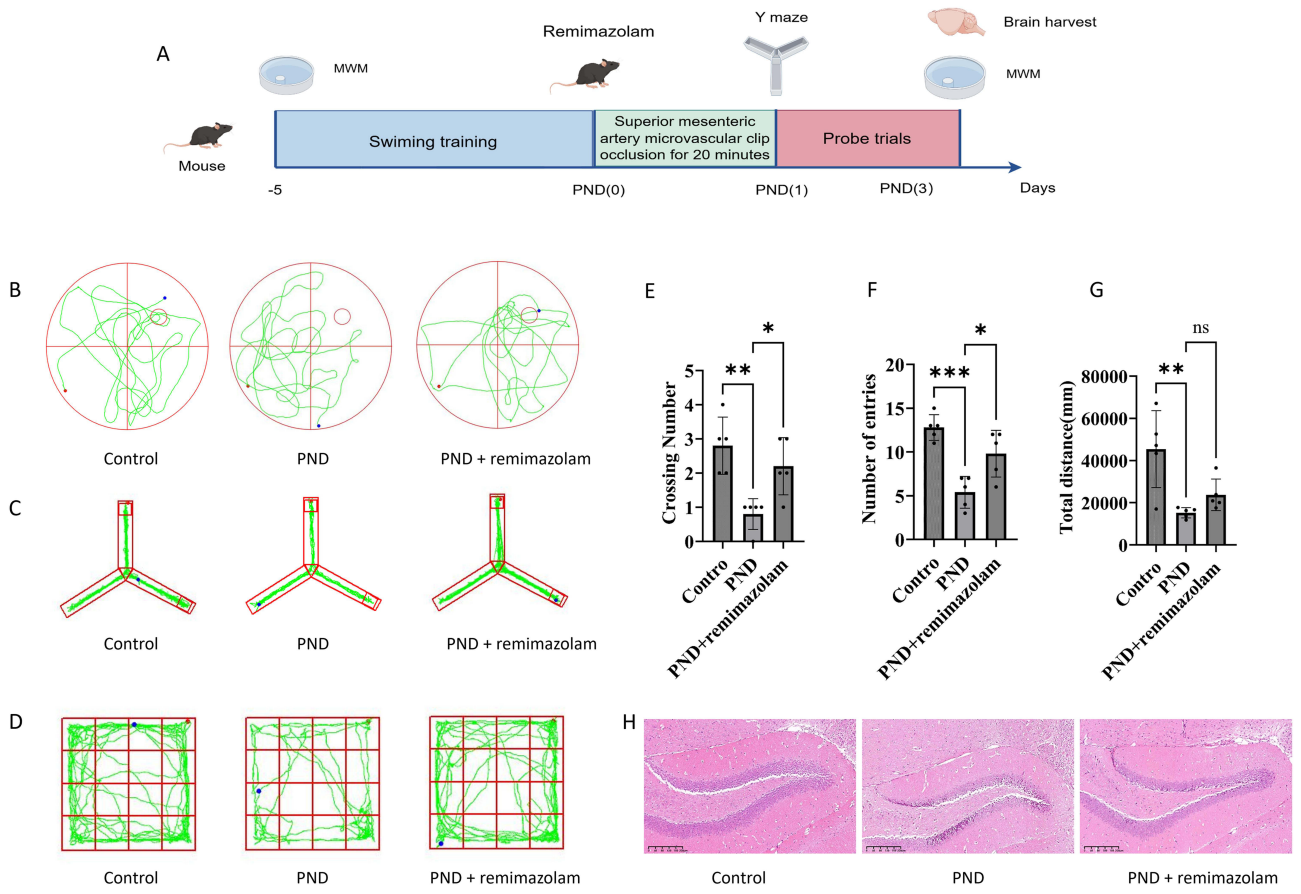

Figure 2 Remimazolam improves cognitive dysfunction in perioperative neurocognitive disorder (PND) mice. (**A**) The experimental flow of animal model construction. (**B**) Representative movement trajectories of each group of mice on the last day of the Morris water maze test (MWM) test. (**C**) Representative movement trajectories of each group of mice on the Y-maze test. (**D**) Representative movement trajectories of each group of mice on the Open field test. (**E**) Number of platform crossings in the MWM test for each group. (**F**) Number of entries in the Y-maze for mice in each group. (**G**) The total distance of each groups in open field test. (**H**) Representative images of HE-stained hippocampal sections from mice in each group. n = 5. *represented $p < 0.05$, **represented $p < 0.01$, ** represented $p < 0.001$, ns represented no significance.

to the PND group (Figure 2F). In the open field test, no statistically significant difference in behavioral performance was observed between the intervention and model groups (Figure 2G). Histological examination revealed that the model group had disorganized hippocampal neuronal architecture, including cellular edema, poorly defined structures, and evident neuronal loss. In contrast, mice in the surgical group treated with remimazolam displayed relatively preserved neuronal morphology, with organized cellular arrangements, clear structural boundaries, and reduced signs of neuronal loss (Figure 2H). Collectively, these findings validate the successful establishment of the PND model and suggest that remimazolam confers a degree of neuroprotective and therapeutic benefit in the context of PND.

With 38 Genes Identified as Candidate Genes

Differential expression analysis identified 357 DEGs1 (343 up-regulated and 14 down-regulated genes) in the model and PND groups (Figure 3A and B), and 323 DEGs2 (149 up-regulated and 174 down-regulated genes) in the intervention and model groups (Figure 3C and D). Subsequently, the enrichment analysis of the DEGs1 indicated that these genes were associated with 1200 GO terms, and included 831 BPs, 170 MFs, and 199 CCs, respectively. These terms encompassed a wide range of functions for instance regulation of synapse structure or activity, neuron to neuron synapse, and actin binding, etc. (Figure 3E and Supplementary Table 2). In total, 42 KEGG pathways were enhanced ($p < 0.05$), and these included endocytosis, cAMP signaling pathway, Amyotrophic lateral sclerosis, and so on (Figure 3F and Supplementary Table 3). And the DEGs2 were associated with 569 GO terms, and included 473 BPs, 37 MFs, and 59 CCs, respectively. These terms encompassed a wide range of functions for instance telencephalon development, neuron

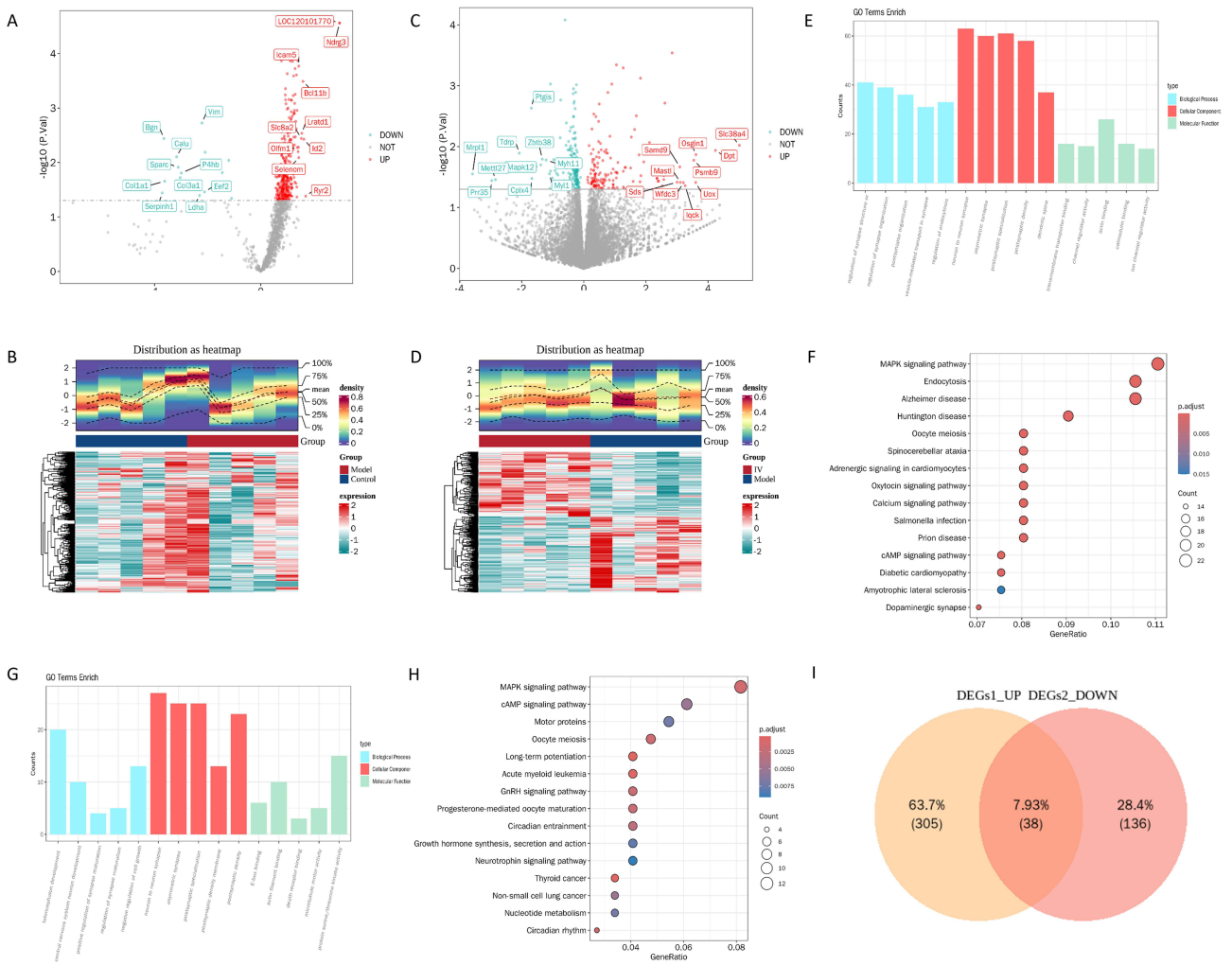

Figure 3 Identification and functional enrichment analysis of differentially expressed genes in the control, PND group, and PND with remimazolam groups. (**A**) Volcano Plot of differentially expressed genes between control and PND group. (**B**) Density Heatmap of differentially expressed genes between control and PND group. (**C**) Volcano Plot of differentially expressed genes between PND group and PND with remimazolam groups. (**D**) Density Heatmap of differentially expressed genes between PND group and PND with remimazolam groups. (**E**) Gene Ontology (GO) comment results of differentially expressed genes between control and PND group (DEGs1). (**F**) KEGG enrichment result of differentially expressed genes between control and PND group (DEGs1). (**G**) GO comment results of differentially expressed genes between PND group and PND with remimazolam groups (DEGs2). (**H**) KEGG enrichment result of differentially expressed genes between PND group and PND with remimazolam groups (DEGs2). (**I**) Venn diagram of the genes exhibiting opposite expression trends in DEGs1 and DEGs2.

to neuron synapse, and actin filament binding, etc. (Figure 3G and Supplementary Table 4). All in all, 112 KEGG pathways were augmented ($p < 0.05$), and these included neurotrophin signaling pathway, long-term potentiation, hypertrophic cardiomyopathy, and so on (Figure 3H and Supplementary Table 5). There were no overlapping genes between the down - regulated genes in DEGs1 and the up - regulated genes in DEGs2. By taking the intersection of the genes with increased expression in DEGs1 and the genes with decreased expression in DEGs2, 38 treatment - related DEGs were obtained, which were used as the candidate genes for this study (Figure 3I). The overlap of genes reflected that drugs might have exerted their effects mainly by inhibiting abnormally upregulated genes in the disease, rather than producing therapeutic effects by activating abnormally downregulated genes in the disease.

Jph3 and Caly Identified as Key Genes

According to these 38 candidate genes, a sum of 34 nodes and 108 sides were shown in a PPI network diagram (No corresponding protein interactions were found for 4 genes) (Figure 4A), the genes Caly, Camk2b, Gria1 and Slc8a2 were found to be strongly linked to other genes. Finally, the results of the MCC algorithm, DMNC algorithm, and MNC algorithm were intersected, and 2 candidate key genes, Jph3 and Caly, were obtained (Figure 4B and C). Subsequently,

https://doi.org/10.2147/DDDT.S541958

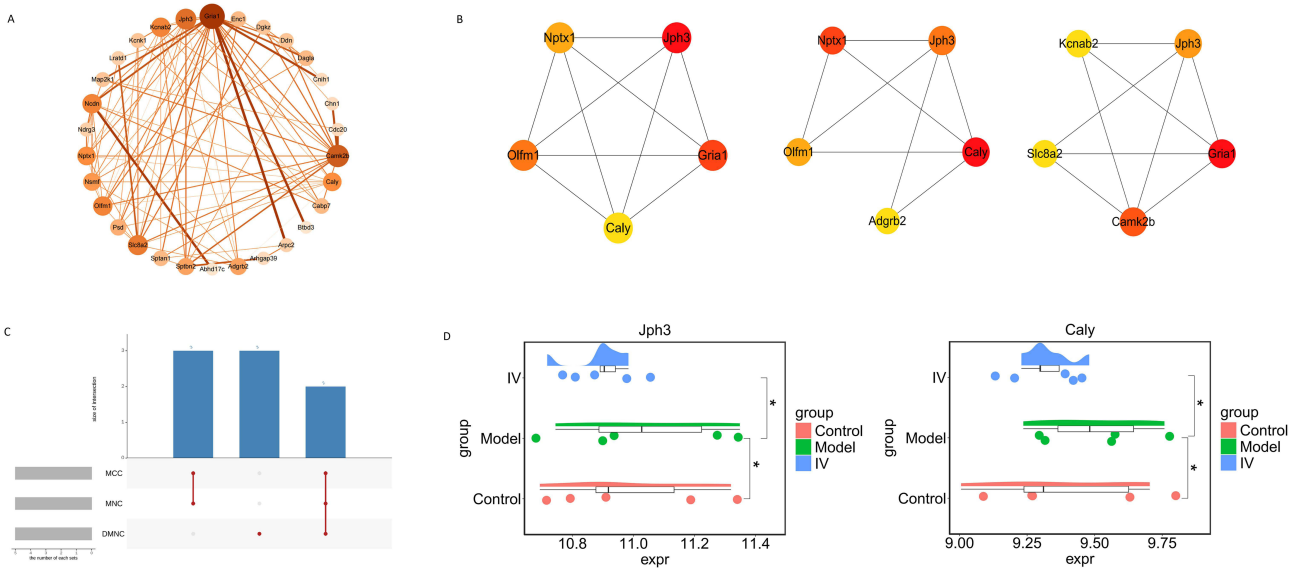

Figure 4 Identification of key genes related to PND treatment. (**A**) Protein-protein interaction network of candidate genes. (**B** and **C**) Intersection analysis of results from the Maximal Clique Centrality (MCC), Density of Maximum Neighborhood Component (DMNC) and Maximum Neighborhood Component (MNC) algorithms identified key genes. (**D**) Expression profiles of *Jph3* and *Caly* across experimental groups. *represented $p < 0.05$.

based on the sequencing data, the candidate key genes Jph3 and Caly were highly expressed in the model group as relative to the PND group, whereas within the intervention group versus the model group, the expression of Jph3 and Caly was lower in the intervention group in contrast to the model group, suggesting that the two genes received the effect of drug intervention, along with a notable disparity in expression among the groups. Therefore, Jph3 and Caly were used as the final key genes (Figure 4D).

Enrichment Pathways of Jph3 and Caly

GSEA revealed several signaling pathways and potential biological mechanisms associated with the 2 key genes. Specifically, in the model group, the Jph3 gene was enriched to 15 pathways, mainly in glutamate receptor binding, structural constituent of cytoskeleton and sulfotransferase activity, while the Caly gene was enriched to 14 pathways, mainly in GABA-gated chloride ion channel activity and tau protein binding. In the intervention group, the Jph3 gene was enriched to 6 pathways, mainly in the pathways intermediate filament-based process and skin development, and the Caly gene was enriched to 37 pathways, mainly in the pathways carbohydrate metabolism and organelle fission (Figure 5A-D and Supplementary Table 6).

Correlations Between Differential Immune Cells and Jph3 as Well as Caly

In the sequencing samples, there were differences in the infiltration ratios of 15 types of immune cells in relation to the model group and the PND group, in addition to between the intervention group and the model group, such as stem cells, stromal cells, and T cells gamma delta (Figure 6A and B). Further examination revealed that there were significant differences in five types of cells, namely dendritic cells, granulocytes, macrophages, CD4 Naive and gamma delta T cells, between the model group and the PND group. However, there were no differentially expressed immune cells between the intervention group and the model group (Figure 6C and D). This indicates that the onset of the disease can lead to changes in the immune microenvironment. These 5 types of immune cells may play a certain role in the disease-developing process, and drug intervention can bring about some improvement to the disease microenvironment. For the group of model establishment and the group of intervention implementation, the inter-relationship analysis for the five differentially immune cells and the key genes revealed that the relationship between the essential genes and the immunocytes with differential expression was faint ($|cor| < 0.3$). The infiltration of immune cells is a dynamic process (for example, the recruitment of immune cells after treatment may fluctuate

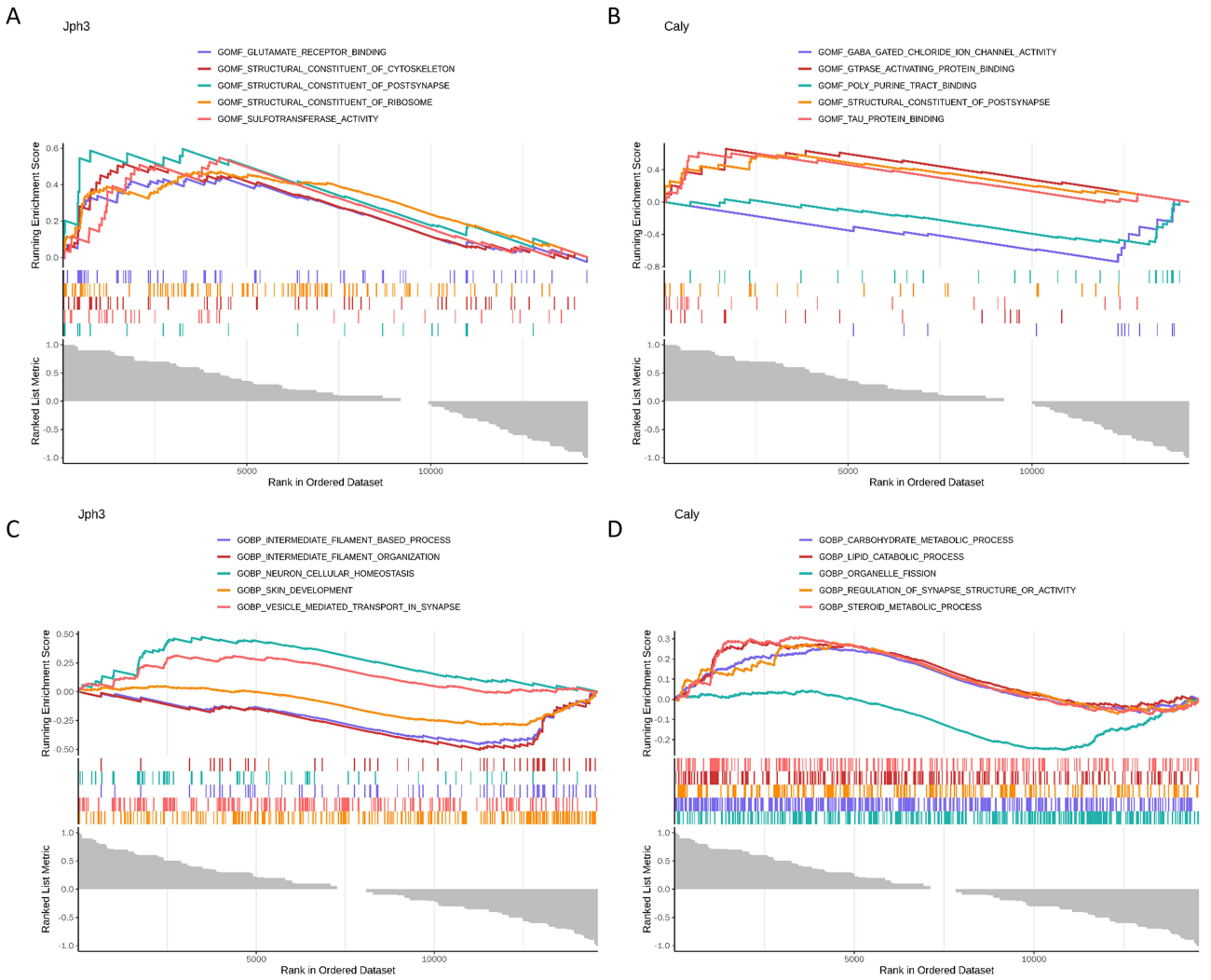

Figure 5 Identification and Gene Set Enrichment Analysis (GSEA) of key genes. (**A–D**) GSEA of two key genes. The top five broken lines were line graphs of the gene Enrichment Score. The vertical axis was the corresponding Running ES. There was a peak value in the line graph, and this peak value was the Enrichment score of this gene set. The genes before the peak were the core genes in this gene set. The horizontal axis represented each gene in this gene set, corresponding to the vertical lines like barcodes in the second part, and each vertical line corresponded to a gene in this gene set. The third part was the distribution graph of the rank values of all genes. The vertical coordinate was the ranked list metric, and the genes were sorted according to their correlation.

over time). If samples are collected at only a single time point, the "window period" for the association between genes and immune cells may be missed. In addition, differences in the composition of immune cells between mice and humans may lead to the failure of the immune regulatory role of key genes shown in the model to be reproduced in clinical data.

Functional Analysis and Network Construction of Key Genes and Molecular Docking

In the GGI network, the 20 genes with the greatest functional similarity to the two genes, Jph3 and Caly, were identified, such as Nsg1, Nsg2, and Drd1. The interaction relationships among these genes included physical interaction, co-expression, co-localization, and shared protein domains. The functions of these genes mainly involve sarcoplasm, regulation of synaptic plasticity, and clathrin binding (Figure 7A). Meanwhile, the m6A modification analysis indicated that Jph3 had higher confidence in the ranges of 20,000–30,000 bp as well as 50,000–60,000 bp compared to Caly, and that Jph3 has more sites that might be modified by methylation (Figure 7B). A total of two miRNAs were predicted to target Jph3, which were mmu-miR-6969-5p and mmu-miR-186-5p (Figure 7C), and the binding energy between Jph3 and remimazolam was −7.1 kcal/mol, and that between Caly and remimazolam was −6.3 kcal/mol, both exhibited good binding energy (Figure 7D).

https://doi.org/10.2147/DDDT.S541958

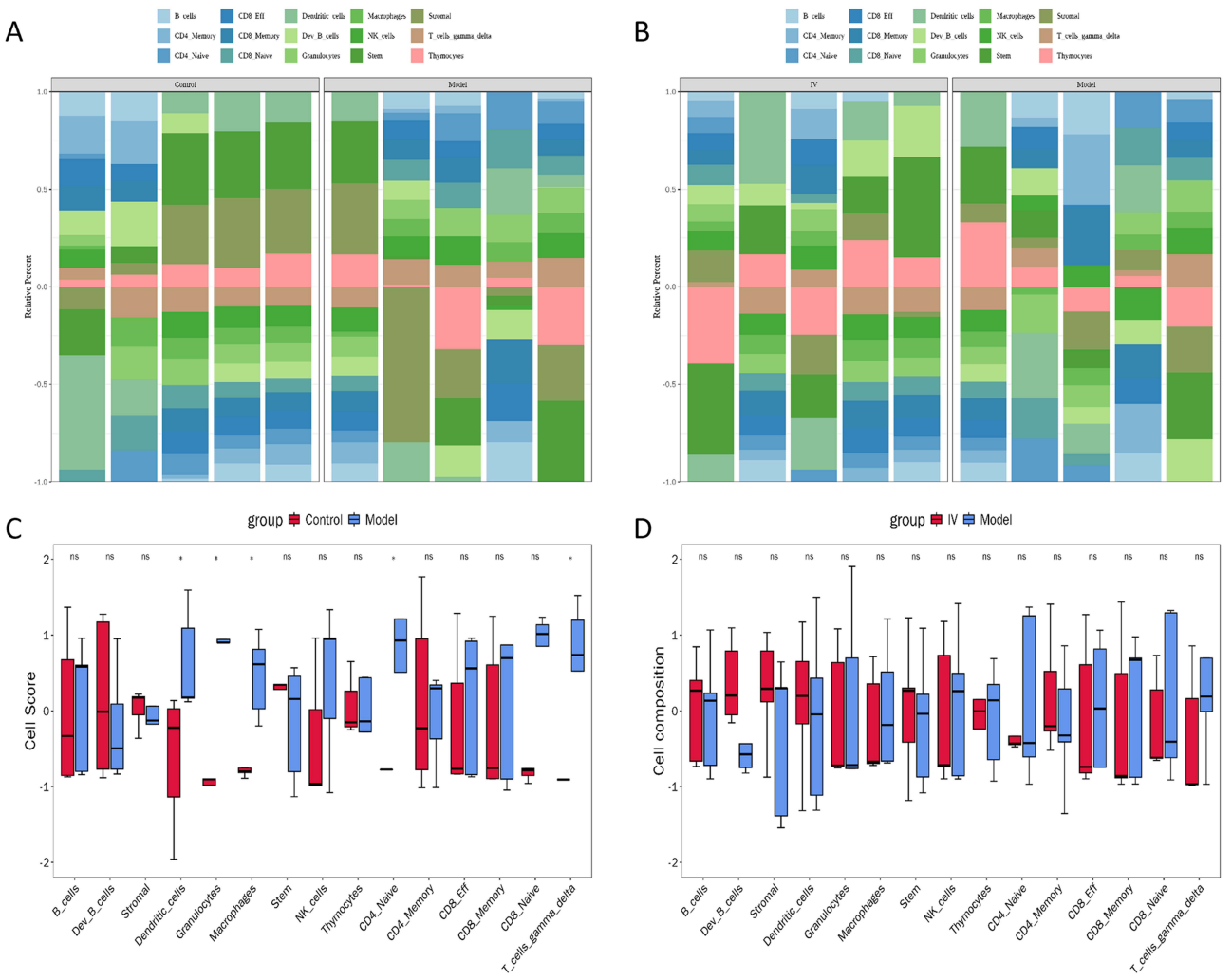

Figure 6 Immune cell infiltration and correlations with key genes. (**A** and **B**) Differential infiltration of immune cell types between control vs model groups and intervention vs model groups. (**C** and **D**) The difference of 15 immune cells between control vs model groups and intervention vs model groups. * represented $p < 0.05$, ns represented No significance.

Expression Verification of Jph3 and Caly

First, a normality test was conducted to verify that the analysis results remained statistically robust under this sample size (Shapiro–Wilk test, $p > 0.05$) (Supplementary Figure 1 and Supplementary Table 7). Furthermore, we observed that the expression extents of Jph3 and Caly in the PND group samples were significantly higher compared to the control samples. In contrast, when contrasted as opposed to the PND group samples, the expression extents of Jph3 and Caly in the PND with remimazolam groups samples had a significant reduction (Figure 8A and B). Moreover, the levels of TNF-α and IL-1β in the serum were significantly elevated in the PND group samples compared to the control group samples, while they were significantly reduced in the PND with remimazolam groups samples compared to the PND group samples (Figure 8C and D). This suggests that treatment with remimazolam can reduce the probability of PND occurrence.

Discussion

This research highlights two important genes (Jph3 and Caly) and possible mechanisms related to remimazolam treatment for PND, such as glutamate receptor interaction, tau protein interaction, and GABA-gated chloride channel function. PND is a prevalent neurological disorder in older patients during the perioperative phase, greatly hindering their recovery and long-term well-being, while placing a heavy burden on families and society.[32] Remimazolam, a new drug with sedative, anesthetic, and hypnotic effects, has gained interest for its anti-inflammatory benefits and possible

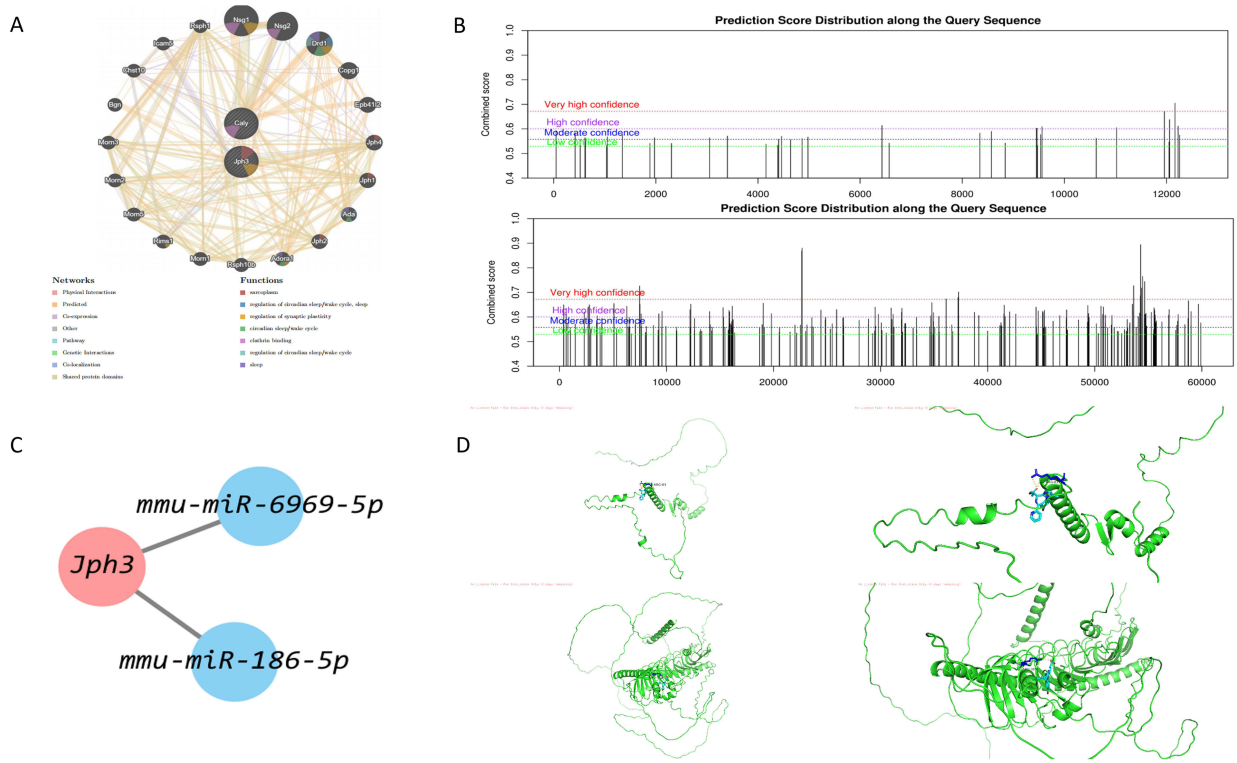

Figure 7 Functional networks and molecular interactions of key genes. (**A**) Gene-gene interaction (GGI) network of *Jph3* and *Caly*. (**B**) M6A modification analysis of *Jph3* and *Caly*. (**C**) Predicted miRNA targets for *Jph3*. (**D**) Molecular docking results of remimazolam with *Jph3* and *Caly*.

effectiveness in reducing PND.[33] Although there is interest, the specific mechanisms of its action are still not completely known. This research utilized remimazolam to address PND caused by surgery and anesthesia in elderly mouse models, and then conducted an extensive analysis of hippocampal transcriptomic data. We initially identified 38 DEGs associated with PND treatment and studied their biological functions and pathways. By analyzing protein-protein interaction (PPI) networks, conducting functional enrichment, examining immune infiltration, and constructing microRNA (miRNA) networks, We discovered two important genes, Jph3 and Caly, and confirmed their expression levels and patterns using quantitative reverse transcription polymerase chain reaction (qRT-PCR).

Using PPI analysis, we discovered two important genes, Jph3 and Caly, that play a role in remimazolam treatment for PND. Jph3 is essential for regulating neurodevelopment and neuronal excitability.[34] The Jph3-encoded protein belongs to the junctophilin family and primarily functions to connect the endoplasmic reticulum membrane with the plasma membrane, creating a membrane junction complex.[35] This complex is crucial for keeping the two membranes close together, forming a structural foundation for communication between the cell membrane and the endoplasmic reticulum.[36] Additionally, Jph3 plays a role in modulating the activity of ryanodine-sensitive calcium release channels, thereby significantly influencing intracellular calcium ion signaling pathways and, consequently, neuronal excitability.[37] Earlier research has identified a strong link between Jph3 and the deterioration of cognitive abilities in several neurodegenerative disorders, especially Huntington's disease type 2 and Alzheimer's disease.[38–40] In mouse models, the Jph3 gene significantly influences neuromuscular control, affecting exploratory behavior, learning, movement, and balance. Abnormal Jph3 expression or deletion alters neurobehavioral and motor functions. In the HDL2 mouse model, CTG/CAG repeat expansion in Jph3 causes progressive motor deficits, neurodegeneration, and ubiquitin-positive nuclear inclusions, impacting behavior and motor skills.[40] Additionally, Jph3 expression affects motor coordination and learning. For instance, Grm1 (crv4) mice lacking the mGlu1 receptor show motor coordination issues linked to mGlu5 receptor overexpression, which may enhance glutamate release and affect these abilities.[40] Notably, a plasma lipidomics and proteomics study of patients progressing from mild cognitive impairment (MCI) to Alzheimer's disease (AD) revealed:

https://doi.org/10.2147/DDDT.S541958

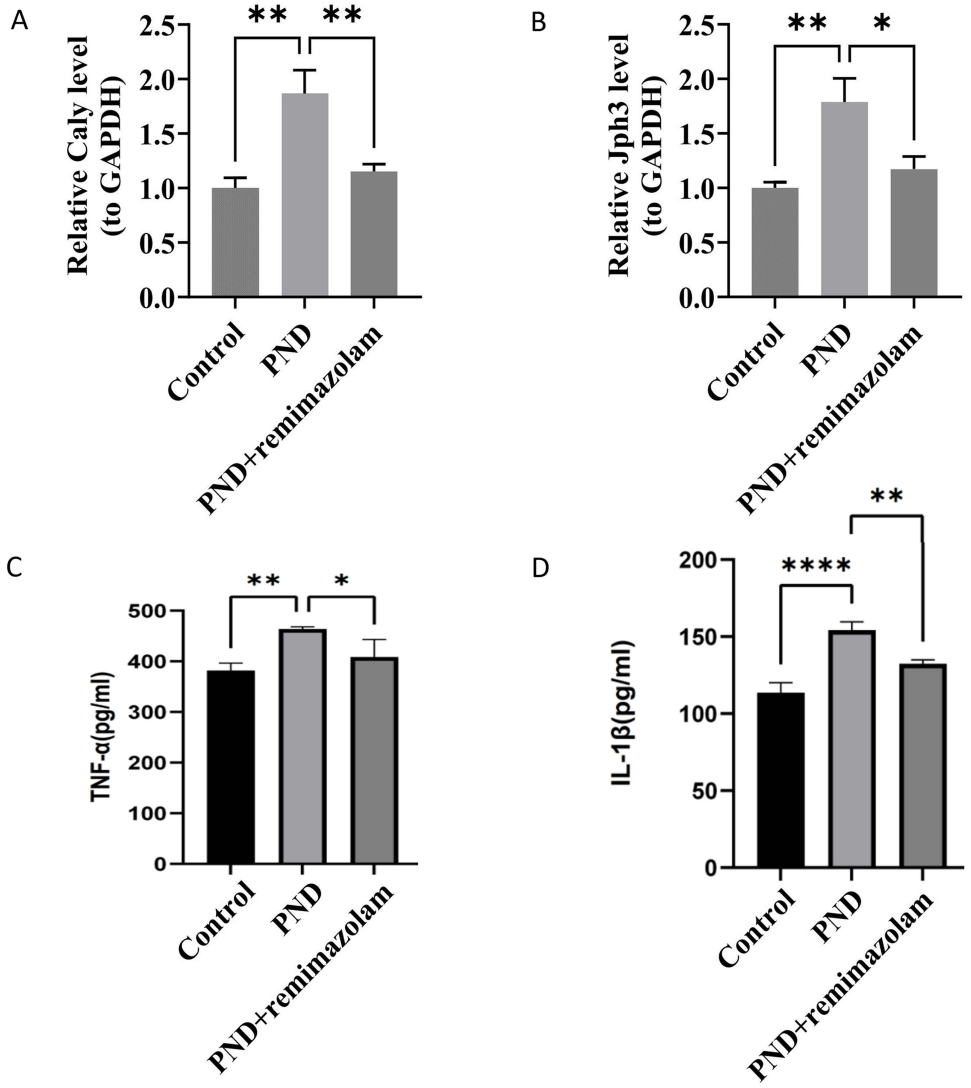

Figure 8 Validation of expression of the mRNA of two key genes. (**A** and **B**) qRT-PCR validation of *Jph3* and *Caly*. (**C** and **D**) Expression levels of TNF-α and IL-1β in the serum of mice from each group. *represented $p < 0.05$, **represented $p < 0.01$, ****represented $p < 0.0001$, n=5.

Jph3 was recognized as a key potential target for the progression from MCI to AD via neuronal and glial inflammatory pathways.[39] These results support our conclusion. Our investigation is the initial one to identify a relationship between Jph3 and PND, indicating that Jph3 expression is reduced post-remimazolam treatment. This suggests that remimazolam's effect on PND might include regulating Jph3 to influence neuronal excitability and the development of neuronal junction membrane structures.

Caly, a neuron-specific vesicle protein, is essential for vesicle trafficking in neurons.[41] It regulates the movement of late endosomes and lysosomal-associated organelles in axons by interacting with motor and vesicle coat proteins, which are essential for synaptic cargo delivery and clearance of damaged macromolecules.[42] Caly collaborates with NEEP21 to influence the movement of glutamate receptors at excitatory synapses, the transport of axonal vesicles, and the handling of amyloid precursor proteins and neuregulin 1.[43] Additionally, Caly binds to calmodulin and affects calcium signaling, which is critical for presynaptic targeting. Its interaction with synaptic vesicle proteins can affect synaptic transmission and neuronal excitability.[44] Consequently, as a neuron-specific vesicle protein, Caly not only plays a pivotal role in vesicle transport within neurons but may also have significant biological implications in neurodevelopment and neurodegenerative diseases. Research indicates that overexpression of the Caly gene in the forebrain of mice leads to several abnormal behaviors, such as increased spontaneous activity, reduced anxiety, and/or impaired harm avoidance.[45]

Furthermore, the interaction between Caly and amyloid precursor protein could affect the pathological development of Alzheimer's disease, highlighting Caly as an important gene in AD, thus reinforcing our findings.[46] This research is the first to show that Galy mRNA levels increase in the hippocampus of PND mice, highlighting the essential role of Galy remimazolam treatment and introducing a new therapeutic target for PND.

Analyses using GSEA and GeneMANIA reveal that two important genes are enriched in pathways like glutamate receptor binding, tau protein binding, and GABA-gated chloride ion channel activity. Glutamate serves as the major excitatory neurotransmitter, with its ionotropic receptors, namely AMPA and NMDA, facilitating synaptic transmission, while its metabotropic receptors (mGluRs) modulate neuronal excitability via G protein-coupled mechanisms.[47,48] Both functional and structural abnormalities in these receptor types have the potential to disrupt synaptic plasticity and neuronal viability; for instance, dysregulation of mGluR3 has been associated with impairments in working memory.[49,50] Research suggests that overactivation of glutamate receptors in the perioperative period may induce neuronal excitotoxicity, resulting in impaired synaptic signaling and subsequent cognitive decline. As a result, the glutamate receptor pathway is strongly associated with cognitive function during the perioperative period.[51] Research indicates that the methylation of Jph3 may affect its expression in neurons, which in turn may affect glutamate receptor function and signalling pathways. Therefore, Jph3 may affect neuronal excitability and synaptic plasticity by regulating the function of glutamate receptors and thus be involved in the pathogenesis of PND.[52]

PND is closely linked to the phosphorylation and unusual buildup of tau protein.[53] Neuronal transport and signaling are impaired by the destabilization of microtubules caused by tau protein's phosphorylation and abnormal accumulation.[54,55] Tau tangles also cause neuroinflammation and stress, exacerbating neuronal damage and death, impairing synaptic transmission and plasticity, and leading to cognitive decline.[56] Gamma-aminobutyric acid (GABA) serves as the primary inhibitory neurotransmitter in the central nervous system, operating via GABA-gated chloride channels to regulate standard neuronal function.[57] Anesthetic drugs like isoflurane and propofol enhance the inhibitory effects of GABA during surgery, which can lead to excessive inhibition and cognitive decline.[58] Dysfunction in GABA-Cl channels is linked to perioperative neuropsychiatric disorders, as anaesthetics can alter these channels, increasing chloride ion influx and disrupting neuronal network regulation, affecting cognitive function.[59] Our research indicated that the Caly gene is mainly associated with pathways involving tau protein binding and the activity of GABA-gated chloride ion channels. This indicates that Caly might play a role in the pathological processes of PND by influencing tau protein phosphorylation/aggregation and altering GABA-mediated chloride channel function. To sum up, two vital genes play a crucial role in regulating glutamate receptor signaling, tau protein metabolism, and GABA-gated chloride ion channel activity pathways, significantly influencing the advancement of PND.

Our study revealed a profound dysregulation of immune cell populations in the hippocampal region of PND mice, with the model group showing marked infiltration of macrophages, gamma delta T cells, dendritic cells and granulocytes compared to controls. These findings collectively suggest that a coordinated pro-inflammatory cascade drives PND pathogenesis. Macrophages are crucial in neuroinflammation and exacerbate neuronal and synaptic problems in perioperative neurocognitive impairment through the overactivation of NLRP3-IL-1β.[60] Removing bone marrow-derived macrophages can stop inflammation in the hippocampus and memory issues following tibial fractures.[61] Studies indicate that monocyte-derived macrophages (MDMs) play a role in the onset of PND in mice suffering from traumatic brain injury (TBI). Pre-anaesthetic treatment with dexmedetomidine (DEX) treatment can reduce MDM infiltration into the hippocampus and ameliorate PND symptoms, indicating that focusing on macrophages could be a treatment strategy for PND.[62] Furthermore, gamma delta T cells, known to induce neuronal hyperexcitability via IL-17 secretion in neurodegenerative contexts, may directly impair synaptic plasticity, a hallmark of PND-related cognitive decline.[63] Dendritic cells, acting as immune orchestrators, potentiate neuroinflammation by activating CD4+ T-cell responses, a mechanism previously implicated in postoperative cognitive dysfunction.[64] In the perioperative phase, the activation of granulocytes can trigger the release of various inflammatory mediators like IL-1β, which may worsen neuroinflammation by activating NLRP3 inflammasomes.[65] This inflammatory response not only affects neuronal function in the hippocampus but can also result in excessive microglial activation, thereby negatively impacting cognitive function.[66] Together, these immune subsets establish a self-reinforcing inflammatory loop within the hippocampus, providing a mechanistic framework for PND progression and potential therapeutic targets.

Nonetheless, it's crucial to acknowledge certain limitations. Initially, the study offers only preliminary validation of these significant genes in a mouse model for remimazolam treatment related to PND. Further investigation using animal and cell studies is required to fully understand the underlying mechanisms. For instance, the generation of Jph3- or Caly-specific knockout mice via the Cre-LoxP system for conditional knockout in hippocampal neurons allows for the examination of their impact on behavioral phenotypes, such as MWM spatial memory and Y-maze spontaneous alternation rate, as well as synaptic functions, including glutamate receptor expression and GABA current intensity, within the PND model. This approach facilitates the elucidation of the roles of these two genes in PND. Concurrently, overexpression experiments can be implemented to ascertain whether these genes are sufficient to ameliorate PND symptoms. Also, the PND mouse model may not completely mirror the human condition due to potential inter-species differences. Consequently, more clinical validation using human samples is required to confirm gene expression and determine the efficacy of remimazolam for treating PND in humans.

Conclusion

Through transcriptomic analysis and experimental validation, this study has identified Jph3 and Caly as critical target genes of remimazolam in the context of PND. The research elucidates their potential mechanisms of action, which involve the regulation of glutamate receptor signaling, tau protein metabolism, and the GABAergic pathway. These findings address a significant research gap concerning the specific target genes and molecular mechanisms of remimazolam in PND, thereby offering a novel theoretical foundation and potential targets for the precise treatment of PND. In conclusion, the identification of key target genes or the repurposing of existing drugs for new applications will enhance our understanding of the pathophysiological processes underlying PND and provide a theoretical basis for future research and therapeutic strategies.

Data Sharing Statement

Data analyzed in this manuscript are publicly available from the Squence Read Archive (https://dataview.ncbi.nlm.nih.gov/object/PRJNA1242678?reviewer=i34c6vdkh200l71po6d7rj1ibu).

Ethics Approval and Consent to Participate

The protocol for the animal study received approval from the Animal Ethics Committee at Guizhou Medical University, under protocol code 2403666, for research involving animals. This research also observed the ARRIVE guidelines (https://arriveguidelines.org).

Author Contributions

All authors made a significant contribution to the work reported, whether that is in the conception, study design, execution, acquisition of data, analysis and interpretation, or in all these areas; took part in drafting, revising or critically reviewing the article; gave final approval of the version to be published; have agreed on the journal to which the article has been submitted; and agree to be accountable for all aspects of the work.

Funding

This research was funded by the National Natural Science Foundation of China (No. 82160224) and the Key Laboratory of Anesthesia and Pain Research at Guizhou Medical University [2024] fy003.

Disclosure

Shilin Yu, Bo Chen and Mei Zhang are co-first authors for this study. The authors declare that they have no competing interests in this work.

References

1. Evered L, Silbert B, Knopman DS, et al. Recommendations for the nomenclature of cognitive change associated with anaesthesia and surgery-2018. *Br J Anaesth*. 2018;121(5):1005–1012. doi:10.1016/j.bja.2017.11.087
2. Moldovan F, Moldovan L. A modeling study for hip fracture rates in romania. *J Clin Med*. 2025;14(9):3162. doi:10.3390/jcm14093162

3. Fidalgo AR. Experimental insights into age-exacerbated cognitive dysfunction after peripheral surgery. *Aging Cell*. 2013;12(3):523–524. doi:10.1111/acel.12066
4. Xin J, Shan W, Li J, et al. Activation of the lateral habenula-ventral tegmental area neural circuit contributes to postoperative cognitive dysfunction in mice. *Adv Sci*. 2022;9(22):e2202228. doi:10.1002/advs.202202228
5. Yang Y, Liu Y, Zhu J, et al. Neuroinflammation-mediated mitochondrial dysregulation involved in postoperative cognitive dysfunction. *Free Radic Biol Med*. 2022;178:134–146. doi:10.1016/j.freeradbiomed.2021.12.004
6. Kong H, Xu LM, Wang DX. Perioperative neurocognitive disorders: a narrative review focusing on diagnosis, prevention, and treatment. *CNS Neurosci Ther*. 2022;28(8):1147–1167. doi:10.1111/cns.13873
7. Bonfante S, Netto MB, de Oliveira Junior AN, et al. Oxidative stress and mitochondrial dysfunction contributes to postoperative cognitive dysfunction in elderly rats dependent on NLRP3 activation. *Metab Brain Dis*. 2024;40(1):1. doi:10.1007/s11011-024-01425-5
8. Yang T, Velagapudi R, Terrando N. Neuroinflammation after surgery: from mechanisms to therapeutic targets. *Nat Immunol*. 2020;21(11):1319–1326. doi:10.1038/s41590-020-00812-1
9. Glumac S, Kardum G, Sodic L, et al. Effects of dexamethasone on early cognitive decline after cardiac surgery: a randomised controlled trial. *Eur J Anaesthesiol*. 2017;34(11):776–784. doi:10.1097/EJA.0000000000000647
10. Duprey MS, Devlin JW, Griffith JL, et al. Association between perioperative medication use and postoperative delirium and cognition in older adults undergoing elective noncardiac surgery. *Anesth Analg*. 2022;134(6):1154–1163. doi:10.1213/ANE.0000000000005959
11. Liao YQ, Min J, Wu ZX, et al. Comparison of the effects of remimazolam and dexmedetomidine on early postoperative cognitive function in elderly patients with gastric cancer. *Front Aging Neurosci*. 2023;15:1123089. doi:10.3389/fnagi.2023.1123089
12. Hu Q, Liu X, Wen C, et al. Remimazolam: an updated review of a new sedative and anaesthetic. *Drug Des Devel Ther*. 2022;16:3957–3974. doi:10.2147/DDDT.S384155
13. Yang M, Liu X, Yang D, et al. Effect of remimazolam besylate compared with propofol on the incidence of delirium after cardiac surgery: study protocol for a randomized trial. *Trials*. 2021;22(1):717. doi:10.1186/s13063-021-05691-x
14. Lee JH, Lee J, Park SH, et al. Comparison between remimazolam and propofol anaesthesia for interventional neuroradiology: a randomised controlled trial. *Anaesth Crit Care Pain Med*. 2024;43(2):101337. doi:10.1016/j.accpm.2023.101337
15. Mao Q, Liang B, Leng Z, et al. Remimazolam ameliorates postoperative cognitive dysfunction after deep hypothermic circulatory arrest through HMGB1-TLR4-NF-κB pathway. *Brain Res Bull*. 2024;217:111086. doi:10.1016/j.brainresbull.2024.111086
16. Zhou Z, Yang Y, Wei Y, et al. Remimazolam attenuates LPS-derived cognitive dysfunction via subdiaphragmatic vagus nerve target α7nAChR-mediated Nrf2/HO-1 signal pathway. *Neurochem Res*. 2024;49(5):1306–1321. doi:10.1007/s11064-024-04115-x
17. Wu T, Li M, Tian L, et al. A modified mouse model of perioperative neurocognitive disorders exacerbated by sleep fragmentation. *Exp Anim*. 2023;72(1):55–67. doi:10.1538/expanim.22-0053
18. Yuan H, Sun D, Ji Y, et al. Pericyte loss impairs the blood-brain barrier and cognitive function in aged mice after anesthesia/surgery. *Brain Res Bull*. 2023;204:110799. doi:10.1016/j.brainresbull.2023.110799
19. Miller-Rhodes P, Kong C, Baht GS, et al. The broad spectrum mixed-lineage kinase 3 inhibitor URMC-099 prevents acute microgliosis and cognitive decline in a mouse model of perioperative neurocognitive disorders. *J Neuroinflammation*. 2019;16(1):193. doi:10.1186/s12974-019-1582-5
20. Wei P, Jia M, Kong X, et al. Human umbilical cord-derived mesenchymal stem cells ameliorate perioperative neurocognitive disorder by inhibiting inflammatory responses and activating BDNF/TrkB/CREB signaling pathway in aged mice. *Stem Cell Res Ther*. 2023;14(1):263. doi:10.1186/s13287-023-03499-x
21. Chen B, Qin G, Xiao J, et al. Transient neuroinflammation following surgery contributes to long-lasting cognitive decline in elderly rats via dysfunction of synaptic NMDA receptor. *J Neuroinflammation*. 2022;19(1):181. doi:10.1186/s12974-022-02528-5
22. Cheon SY, Koo B-N, Kim SY, et al. Scopolamine promotes neuroinflammation and delirium-like neuropsychiatric disorder in mice. *Sci Rep*. 2021;11(1):8376. doi:10.1038/s41598-021-87790-y
23. Gustavsson EK, Zhang D, Reynolds RH, et al. ggtranscript: an R package for the visualization and interpretation of transcript isoforms using ggplot2. *Bioinformatics*. 2022;38(15):3844–3846. doi:10.1093/bioinformatics/btac409
24. Love MI, Huber W, Anders S. Moderated estimation of fold change and dispersion for RNA-seq data with DESeq2. *Genome Biol*. 2014;15(12):550. doi:10.1186/s13059-014-0550-8
25. Gu Z, Eils R, Schlesner M. Complex heatmaps reveal patterns and correlations in multidimensional genomic data. *Bioinformatics*. 2016;32(18):2847–2849. doi:10.1093/bioinformatics/btw313
26. Wu T, Hu E, Xu S, et al. clusterProfiler 4.0: a universal enrichment tool for interpreting omics data. *Innovation*. 2021;2(3):100141. doi:10.1016/j.xinn.2021.100141
27. Ahmed M, Sallari RC, Guo H, et al. Variant set enrichment: an R package to identify disease-associated functional genomic regions. *BioData Min*. 2017;10:9. doi:10.1186/s13040-017-0129-5
28. Chen H, Boutros PC. VennDiagram: a package for the generation of highly-customizable Venn and Euler diagrams in R. *BMC Bioinformatics*. 2011;12:35. doi:10.1186/1471-2105-12-35
29. Shannon P, Markiel A, Ozier O, et al. Cytoscape: a software environment for integrated models of biomolecular interaction networks. *Genome Res*. 2003;13(11):2498–2504. doi:10.1101/gr.1239303
30. Sturm G, Finotello F, Petitprez F, et al. Comprehensive evaluation of transcriptome-based cell-type quantification methods for immuno-oncology. *Bioinformatics*. 2019;35(14):i436–i445. doi:10.1093/bioinformatics/btz363
31. Duricki DA, Soleman S, Moon LD. Analysis of longitudinal data from animals with missing values using SPSS. *Nat Protoc*. 2016;11(6):1112–1129. doi:10.1038/nprot.2016.048
32. Eckenhoff RG, Maze M, Xie Z, et al. Perioperative neurocognitive disorder: state of the preclinical science. *Anesthesiology*. 2020;132(1):55–68. doi:10.1097/ALN.0000000000002956
33. Wen T, Wen J, Yao C. Remimazolam inhibits postoperative cognitive impairment after cardiopulmonary bypass by alleviating neuroinflammation and promoting microglia M2 polarization. *Brain Res*. 2024;1838:148975. doi:10.1016/j.brainres.2024.148975
34. Bourinaris T, Athanasiou A, Efthymiou S, et al. Allelic and phenotypic heterogeneity in Junctophillin-3 related neurodevelopmental and movement disorders. *Eur J Hum Genet*. 2021;29(6):1027–1031. doi:10.1038/s41431-021-00866-1

35. Perni S, Beam K. Junctophilins 1, 2, and 3 all support voltage-induced Ca2+ release despite considerable divergence. *J Gen Physiol*. 2022;154(9). doi:10.1085/jgp.202113024
36. Wilburn B, Rudnicki D, Zhao J, et al. An antisense CAG repeat transcript at JPH3 locus mediates expanded polyglutamine protein toxicity in Huntington's disease-like 2 mice. *Neuron*. 2011;70(3):427–440. doi:10.1016/j.neuron.2011.03.021
37. Lehnart SE, Wehrens XHT. The role of junctophilin proteins in cellular function. *Physiol Rev*. 2022;102(3):1211–1261. doi:10.1152/physrev.00024.2021
38. Bilal H, Harding IH, Stout JC. The temporal dynamics of mood and their association with depressive symptoms in Huntington's disease. *J Affect Disord*. 2023;328:22–28. doi:10.1016/j.jad.2023.02.035
39. Gómez-Pascual A, Naccache T, Xu J, et al. Paired plasma lipidomics and proteomics analysis in the conversion from mild cognitive impairment to Alzheimer's disease. *Comput Biol Med*. 2024;176:108588. doi:10.1016/j.compbiomed.2024.108588
40. Anderson DG, Krause A, Margolis RL, et al. *Huntington Disease-Like 2, in Genereviews(®)*.Adam MP,Editors.University of Washington, Seattle Copyright © 1993-2025, University of Washington, Seattle. GeneReviews is a registered trademark of the University of Washington, Seattle. All rights reserved:Seattle (WA);1993
41. Shi L, Muthusamy N, Smith D, et al. Dynein binds and stimulates axonal motility of the endosome adaptor and NEEP21 family member, calcyon. *Int J Biochem Cell Biol*. 2017;90:93–102. doi:10.1016/j.biocel.2017.07.005
42. Shi L, Hines T, Bergson C, et al. Coupling of microtubule motors with AP-3 generated organelles in axons by NEEP21 family member calcyon. *Mol Biol Cell*. 2018;29(17):2055–2068. doi:10.1091/mbc.E18-01-0007
43. Muthusamy N, Chen Y-J, Yin D-M, et al. Complementary roles of the neuron-enriched endosomal proteins NEEP21 and calcyon in neuronal vesicle trafficking. *J Neurochem*. 2015;132(1):20–31. doi:10.1111/jnc.12989
44. Müller HK, Kragballe M, Fjorback AW, et al. Differential regulation of the serotonin transporter by vesicle-associated membrane protein 2 in cells of neuronal versus non-neuronal origin. *PLoS One*. 2014;9(5):e97540. doi:10.1371/journal.pone.0097540
45. Holy M, Brautigan DL. Calyculin A from Discodermia calyx is a dual action toxin that blocks calcium influx and inhibits protein Ser/Thr phosphatases. *Toxins*. 2012;4(10):940–954. doi:10.3390/toxins4100940
46. Hamarsha A, Balachandran K, Sailan AT, et al. Predicting key genes and therapeutic molecular modelling to explain the association between porphyromonas gingivalis (P. gingivalis) and Alzheimer's Disease (AD). *Int J Mol Sci*. 2023;24(6):5432. doi:10.3390/ijms24065432
47. Reiner A, Levitz J. Glutamatergic signaling in the central nervous system: ionotropic and metabotropic receptors in concert. *Neuron*. 2018;98(6):1080–1098. doi:10.1016/j.neuron.2018.05.018
48. Zhang S, Edwards TN, Chaudhri VK, et al. Nonpeptidergic neurons suppress mast cells via glutamate to maintain skin homeostasis. *Cell*. 2021;184(8):2151–2166.e16. doi:10.1016/j.cell.2021.03.002
49. Revett TJ, Baker GB, Jhamandas J, et al. Glutamate system, amyloid ß peptides and tau protein: functional interrelationships and relevance to Alzheimer disease pathology. *J Psychiatry Neurosci*. 2013;38(1):6–23. doi:10.1503/jpn.110190
50. Jin LE, Wang M, Galvin VC, et al. mGluR2 versus mGluR3 Metabotropic Glutamate Receptors in Primate Dorsolateral Prefrontal Cortex: postsynaptic mGluR3 Strengthen Working Memory Networks. *Cereb Cortex*. 2018;28(3):974–987. doi:10.1093/cercor/bhx005
51. Tse V. Astrocytic control of glutamate spillover and extrasynaptic NMDA receptor activation: implications for neurodegenerative disorders. *J Neurosci*. 2024;44(21):e0083242024. doi:10.1523/JNEUROSCI.0083-24.2024
52. Huang Y. Methylation-associated inactivation of JPH3 and its effect on prognosis and cell biological function in HCC. *Mol Med Rep*. 2022;25(4):1–3.
53. Menuet C, Borghgraef P, Voituron N, et al. Isoflurane anesthesia precipitates tauopathy and upper airways dysfunction in pre-symptomatic Tau. P301L mice: possible implication for neurodegenerative diseases. *Neurobiol Dis*. 2012;46(1):234–243. doi:10.1016/j.nbd.2012.01.012
54. Wang Y, Mandelkow E. Tau in physiology and pathology. *Nat Rev Neurosci*. 2016;17(1):5–21. doi:10.1038/nrn.2015.1
55. Andreone BJ, Larhammar M, Lewcock JW. Cell death and neurodegeneration. *Cold Spring Harb Perspect Biol*. 2020;12(2):a036434. doi:10.1101/cshperspect.a036434
56. Chiang ACA, Huo X, Kavelaars A, et al. Chemotherapy accelerates age-related development of tauopathy and results in loss of synaptic integrity and cognitive impairment. *Brain Behav Immun*. 2019;79:319–325. doi:10.1016/j.bbi.2019.04.005
57. Liang D, Zhou L, Zhou H, et al. A GABAergic system in atrioventricular node pacemaker cells controls electrical conduction between the atria and ventricles. *Cell Res*. 2024;34(8):556–571. doi:10.1038/s41422-024-00980-x
58. Fu N, Wang Y, Zhu R, et al. Bicuculline and bumetanide attenuate sevoflurane-induced impairment of myelination and cognition in young mice. *ACS Chem Neurosci*. 2023;14(6):1146–1155. doi:10.1021/acschemneuro.2c00764
59. Khanna A, Walcott BP, Kahle KT. Limitations of current GABA agonists in neonatal seizures: toward GABA modulation via the targeting of neuronal Cl(-) transport. *Front Neurol*. 2013;4:78. doi:10.3389/fneur.2013.00078
60. Chen K, Hu Q, Xie Z, et al. Monocyte NLRP3-IL-1 β hyperactivation mediates neuronal and synaptic dysfunction in perioperative neurocognitive disorder. *Adv Sci*. 2022;9(16):e2104106. doi:10.1002/advs.202104106
61. Degos V, Vacas S, Han Z, et al. Depletion of bone marrow-derived macrophages perturbs the innate immune response to surgery and reduces postoperative memory dysfunction. *Anesthesiology*. 2013;118(3):527–536. doi:10.1097/ALN.0b013e3182834d94
62. Kii N, Sawada A, Yoshikawa Y, et al. Dexmedetomidine ameliorates perioperative neurocognitive disorders by suppressing monocyte-derived macrophages in mice with preexisting traumatic brain injury. *Anesth Analg*. 2022;134(4):869–880. doi:10.1213/ANE.0000000000005699
63. Wo J, Zhang F, Li Z, et al. The role of gamma-delta T cells in diseases of the central nervous system. *Front Immunol*. 2020;11:580304. doi:10.3389/fimmu.2020.580304
64. Garré JM, Silva HM, Lafaille JJ, et al. CX3CR1(+) monocytes modulate learning and learning-dependent dendritic spine remodeling via TNF-α. *Nat Med*. 2017;23(6):714–722. doi:10.1038/nm.4340
65. Que YY, Zhu T, Zhang F-X, et al. Neuroprotective effect of DUSP14 overexpression against isoflurane-induced inflammatory response, pyroptosis and cognitive impairment in aged rats through inhibiting the NLRP3 inflammasome. *Eur Rev Med Pharmacol Sci*. 2020;24(12):7101–7113. doi:10.26355/eurrev_202006_21704
66. Sun XY, Zheng T, Yang X, et al. HDAC2 hyperexpression alters hippocampal neuronal transcription and microglial activity in neuroinflammation-induced cognitive dysfunction. *J Neuroinflammation*. 2019;16(1):249. doi:10.1186/s12974-019-1640-z